098639

ELSEVIER

Journal of Contaminant Hydrology 54 (2002) 59–80

JOURNAL OF
Contaminant
Hydrology

www.elsevier.com/locate/jconhyd

Investigation of the vadose zone using barometric pressure cycles

Donald A. Neeper *

Science and Engineering Associates, Inc., 3205 Richards Lane, Suite A, Santa Fe, NM 87505, USA

Received 21 November 2000; received in revised form 4 June 2001; accepted 12 June 2001

Abstract

This paper documents a technique for investigating one-dimensional airflow in the vadose zone. Variations in pore gas pressures resulting from barometric cycles were measured at depths as great as 180 m in several gas monitoring wells. The data were transformed to the frequency domain, enabling comparison with closed-form analytic expressions of one-dimensional pressure transport in layered porous media. The data reveal evidence for vertical fracture flow that was not apparent from in situ measurements of permeability. The data also reveal that the basalt underlying the site at depths greater than 100 m has permeability exceeding 1000 darcies, and is vented to the atmosphere at an estimated distance of a few kilometers from the site. © 2002 Elsevier Science B.V. All rights reserved.

Keywords: Soil venting; Soil vapor extraction; Atmospheric pressure; Vadose zone; Harmonic analysis; Barometric pumping

1. Introduction

This paper describes an investigation of the vadose zone by measurement of its transmission of barometric pressure variations, particularly as those variations are resolved into periodic components. The investigation was conducted as preparation for either active or passive soil vapor extraction in ash flow tuffs, where it was feared that subsurface airflow might occur mainly in fractures, and consequently be ineffective for removal of volatile contaminants. The purpose of this paper is to illustrate a

* WGI/PMC/SEA Los Alamos Project Office, 2237 Trinity Drive, Bldg. 2, Los Alamos, NM 87544, USA. Fax: +1-505-662-1398.

E-mail address: dneeper@aol.com (D.A. Neeper).

0169-7722/02/$ - see front matter © 2002 Elsevier Science B.V. All rights reserved.
PII: S0169-7722(01)00146-2

30852

technique for investigation of hydrologic properties and airflow. A subsequent paper will document the use of harmonic analysis for the prediction of barometric airflow in open boreholes.

Other investigators have studied the propagation of barometric pressure variations in the vadose zone. Weeks (1978) inferred the pneumatic diffusivity of soil layers above an impermeable boundary by measuring the pressure transient at several depths induced by a several-hour synoptic weather event. Burkhard et al. (1987) estimated the pneumatic diffusivity of chimneys resulting from underground nuclear explosions. Shan (1995) presented analytical solutions for interpreting subsurface pressure measurements. Rousseau et al. (1999) reported extensive measurements and interpretation of subsurface pressure variations at the proposed Yucca Mountain nuclear waste repository. Ahlers et al. (1999) presented the use of one-, two-, and three-dimensional models in interpreting subsurface pressure measurements at Yucca Mountain. Ellerd et al. (1999) discussed the subsurface propagation of barometric pressure variations in relation to passive vapor extraction. The influence of barometric pressure changes has also been studied in regard to airflow in caves (Lewis, 1991), to radon migration into buildings (Robinson et al., 1997), and to the transport of vapors in soils (Massmann and Farrier, 1992).

2. Geologic setting

The investigation was conducted at Mesita del Buey, a narrow finger mesa at Los Alamos National Laboratory, New Mexico, USA. Numerous boreholes have been drilled at the site to obtain core samples for analysis of geohydrologic properties and possible contaminants. Some of those boreholes were completed as monitoring wells for a subsurface vapor plume of volatile organic compounds. These wells proved useful for monitoring of subsurface gas pressure as well as pore gas content. The monitoring wells discussed in this paper are shown schematically in Fig. 1, which presents a vertical cross-section through the mesa at a plane containing Well 1004. Fig. 1 shows the projections of other relevant wells at the plane.

Mesita del Buey trends northwest–southeast. Approximately 0.2 m of surface soil overlies a series of ash-flow tuffs that form the canyon walls (Broxton et al., in preparation; Broxton and Reneau, 1995). From youngest to oldest, the general stratigraphic setting includes: the Quaternary age Tshirege member of the Bandelier Tuff (Qbt); the Cerro Toledo interval (Qct); the Otowi member of the Bandelier Tuff (Qbo, which includes the Guaje pumice bed); and the Quaternary-Tertiary Cerros del Rio basalt (QTb). The stratigraphy is divided into subunits. Subunit Qbt2 is the cap rock, which is moderately welded and more fractured than the underlying tuffs. Most fractures are nearly vertical, although some horizontal and low-angle fractures are present. Many of the fractures extend into the upper part of subunit Qbt1v, indicated as $Qbt1v_u$. Qbt1 is a succession of ash-flow tuffs, divided into an upper devitrified and vapor-phase altered tuff (Qbt1v), and a lower glassy tuff (Qbt1g). Qbt1v is further divided into an upper subunit ($Qbt1v_u$) and a basal, resistant subunit ($Qbt1v_c$, called "the colonnade") having abundant vertical fractures and smooth dihedral surfaces on cliff faces. Some fractures persist downward into the subunit Qbt1g. Data presented later in this paper indicate that the

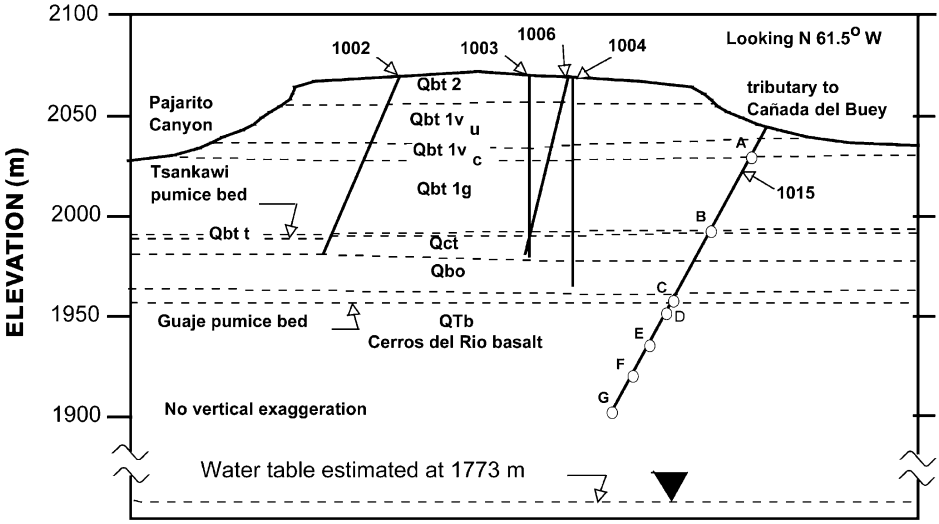

Fig. 1. Diagram of the stratigraphy and projections of wells on a plane containing Well 1004. Ports A–G of Well 1015 are indicated. Well 1016 is approximately parallel to Well 1015, and is not shown.

fractures result in a large vertical permeability. The Tsankawi pumice bed (Qbt t) varies in thickness from less than 1 to 2 m. The Cerro Toledo interval (Qct) consists of alluvial material varying from silt to cobbles. The Otowi Member of the Bandelier Tuff (Qbo) consists of an ash-flow tuff and the Guaje pumice bed, which is a basal air-fall subunit. Between the Guaje pumice bed and the Cerros del Rio basalt is a thin, moist layer of unconsolidated sediment, which is 0.5 m thick in Well 1016 but is 2.3 m thick in the nearby parallel Well 1015, where the top of the basalt is 10 m lower in elevation. The character of the basalt varies from massive to coarsely vesicular intervals, with isolated rubble zones.

3. Instrumentation

Wells 1002, 1003, 1004, and 1006 were drilled with an auger. Wells 1002 and 1006 were slanted with the intent of intersecting some of the vertical fractures. The surface casing extended to 9-m depth in these wells because these holes were intended for eventual use as vapor extraction wells, and applied vacuum was not wanted at depths less than 9 m. Porosity and other hydraulic properties were measured in a laboratory on selected core samples of Wells 1002, 1003, and 1006. Before completion as monitoring wells, the air permeability was measured in situ in each of these three boreholes at about 25 different depths with a straddle packer apparatus. Boreholes 1002, 1003, 1004, and 1006 were completed as temporary vapor and pressure monitoring wells by deployment of inflated everting membrane liners, shown schematically in Fig. 2. The crank and reel assembly for deployment and retraction of the liner was removed after installation. (Liners are available

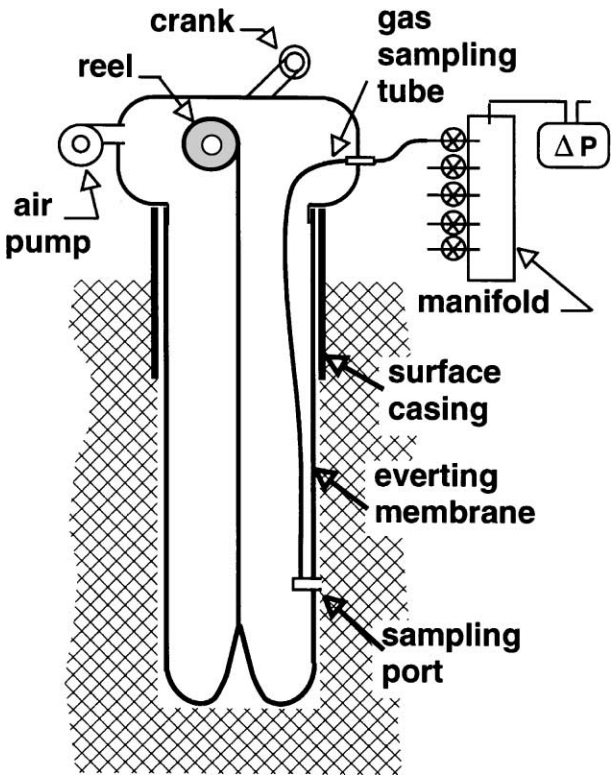

Fig. 2. Schematic diagram of a monitoring well with a retractable membrane liner and monitoring apparatus. One of twelve sampling ports is shown. The horizontal scale is exaggerated.

from Flexible Liner Underground Technologies, 6 Easy St., Santa Fe, NM 87501 USA.) Each membrane-lined well had a small, photovoltaic-powered air pump that maintained pressure to hold the membrane against the borehole wall. The membrane liners operated successfully for several years, and were usually still operating when retracted for decommissioning. Each liner was constructed with 12 sampling tubes leading to 12 ports (labeled A through L) at depths selected by inspection of drill cores. Pressure could be measured or a gas sample could be withdrawn from any port.

Wells 1015 and 1016 were drilled by an air-rotary rig with the intent of exploring the basalt. They were completed as permanent vapor monitoring wells with seven ports each. Some of the ports proved unsatisfactory for pressure monitoring, presumably due to imperfect seals in peristaltic pumps attached to the ports for sampling any water that might gather in the basalt.

For pressure measurements, the sampling tubes of one or more wells were connected to individual solenoid valves on a manifold, which in turn led to a differential pressure transducer that sensed the difference between manifold pressure and atmospheric pressure. Atmospheric pressure was monitored by a separate absolute pressure transducer. Subsur-

face pressures were inferred by adding the differential measurement to the measured value of atmospheric pressure. The transducers were mounted in a temperature-controlled enclosure to eliminate generation of small artificial periodic signals caused by diurnal ambient temperature cycles. Pressures, various temperatures, and diagnostic data were recorded by an automatic data unit at 45-min intervals.

This system did not directly measure subsurface pressures, but rather measured the pressure at each subsurface port minus the head produced by the vertical column of air in the sampling tube. Presumably, this head was the same as that of the air column in the connected porosity of the ground. Thus, the system measured all pressures as referred to ground level, which is appropriate for harmonic analysis that depends only on the changes of pressure with time, not on the static head at each port. This system is more convenient than burying an absolute pressure transducer at each depth in the ground, as was done by Rojstaczer and Tunks (1995).

4. Analytical method

As noted by Fukuda (1955), the propagation of small variations of gas pressure in a porous medium is described by a diffusion equation in pressure, analogous to temperature or chemical diffusion:

$$\frac{\partial^2 P}{\partial y^2} = \frac{\mu\theta}{kP_{00}} \frac{\partial P}{\partial t}, \tag{1}$$

in which P represents pressure, which varies only slightly from the constant average pressure, P_{00} (notation is defined at the end of this paper). The so-called "pneumatic diffusivity" is $kP_{00}/\mu\theta$. Weeks (1978) showed that the diffusivities of soil layers could be inferred from Eq. (1) by measurement of subsurface pressures during a several-hour transient of barometric pressure. Weeks used a numerical trial-and-error procedure to fit his data to Eq. (1). Rojstaczer and Tunks (1995) presented the solution of Eq. (1) for boundary conditions representing a periodic pressure variation at ground surface and an impermeable lower boundary, and attempted to infer a single value of the effective diffusivity by measuring the time history of pressure at two different depths. Shan (1995) presented a method for inferring the diffusivity of a layer by measuring the pressure history at each boundary and at the middle. Rousseau et al. (1999) used Weeks' method. To infer the soil diffusivity from pressure measurements, Ahlers et al. (1999) iterated numerical simulations until the calculated pressure history became acceptably close to the measured history.

In the work reported here, the pressure history was transformed to a set of periodic components (the frequency domain) because periodic solutions to Eq. (1) are known for a variety of plane and cylindrical geometric configurations (Carslaw and Jaeger, 1959). This investigation was designed to use the well-defined periods of the atmospheric tides as a precise source of signals for the investigation of the pneumatic diffusivity. Daily variations in atmospheric pressure, called atmospheric tides (or S-tides) are caused by absorption of solar energy in the atmosphere. These regular variations have periods of integral fractions

of one solar day (that is, periods of 1 day, 1/2 day, 1/3 day, etc.). The resulting daily peak-to-peak pressure variation is usually a few millibars (few hundred Pa) at mid latitudes. In addition to these perfectly periodic cycles, synoptic weather systems cause larger pressure variations at irregular intervals of several days. Within certain limits, these synoptic variations can also be represented by periodic components. Ahlers et al. (1999) summarized barometric pressure variations. Chapman and Lindzen (1970) present details on the atmospheric tides.

In data analysis, the Fast Fourier Transform (FFT) algorithm was used to transform a selected set of measured pressure-time pairs to a set of amplitude-phase pairs, so that the resulting pressure variation was represented by a set of amplitudes and phases at harmonic intervals of frequency (or period). Measurements were recorded at intervals of 45 min (32 measurements/day) and data were transformed to the frequency domain from carefully selected windows of 32 or 64 days. The 45-min data interval, combined with these window widths, allowed particular output periods of the FFT to exactly equal the harmonics of one 24-h day, thereby closely matching the periods of the atmospheric S-tides. Details of the data treatment are presented in Appendix A.

In an infinitely deep soil with uniform permeability and porosity, the solution to Eq. (1) for a single angular frequency, ω_n, is

$$\mathbf{P}_n = P_{n0}\mathrm{e}^{-\beta y}\mathrm{e}^{i(\omega_n t+\phi_n)}, \tag{2}$$

in which the exponential decay parameter, β, and the phase shift, ϕ_n, are given by

$$\beta = \sqrt{\frac{\omega_n \mu\theta}{2kP_{00}}}\,; \qquad \phi_n = -\beta y. \tag{3}$$

In more generality, within a layer of arbitrary thickness, having arbitrary boundary conditions, the solution to Eq. (1) is

$$\mathbf{P}_n = P_{n0}\{\mathbf{C}_1\sinh[\,\beta y(1+i)] + \mathbf{C}_2\cosh[\,\beta y(1+i)]\}\mathrm{e}^{i\omega_n t}, \tag{4}$$

in which $\mathbf{C}_1$ and $\mathbf{C}_2$ are complex constants determined by the boundary conditions. The magnitude of the amplitude ratio, $|\mathbf{P}_n/P_{n0}|$ indicates the attenuation of the pressure. The phase shift, ϕ_n, indicates the delay in time as a component of pressure at frequency ω_n is transmitted to a location at depth y within a layer.

The propagation of a periodic pressure through a series of layers, each layer having a fixed permeability and porosity, can be calculated by successive multiplication of a set of 2×2 complex matrices (Carslaw and Jaeger, 1959, p. 109). Each matrix represents one layer. A numerical layer model was constructed to calculate the amplitude ratios and phase shifts at the depths of ports for frequencies (periods) of interest, using input values for the permeability, porosity, and thickness of each layer.

Fig. 3a presents a sample of time-series pressure data for the atmosphere and four ports of Well 1004. From days 357 to 363, the atmospheric pressure undergoes a slow decline, with obvious peaks due to the diurnal and semi-diurnal S-tides. During 3 days starting at day 363, a low pressure associated with a storm occurs. Winter weather at this location

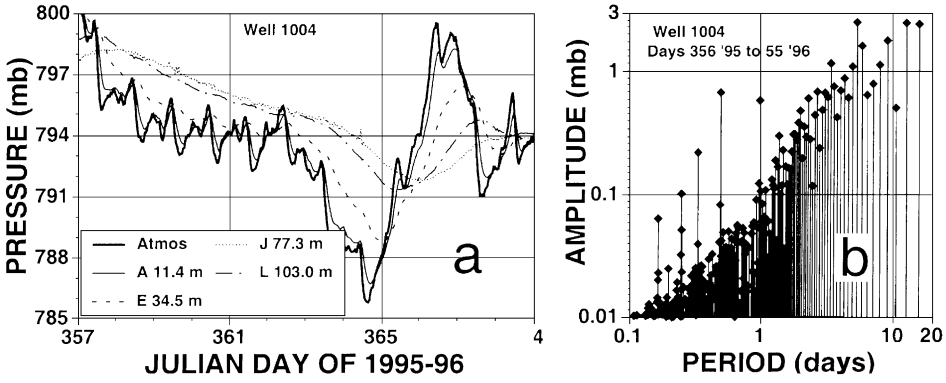

Fig. 3. (a) Pressure versus time at ground surface and at four depths of Well 1004. (b) Amplitude versus period of atmospheric pressure from a 64-day data window that includes the interval shown in (a). The 1-day S-tide and its harmonics rise above the background.

typically has low-pressure events at intervals of approximately 10 days. During the summer, low-pressure events occur less frequently. At the 11.4-m depth of Port A, the pressure closely follows the barometric changes with little delay, and the diurnal cycles are obvious. The diurnal cycles are less obvious at Port E (34.5-m depth) and are not apparent at the deeper ports, which respond to barometric changes with delay times of approximately 1 day.

As shown in Fig 3a, Port L responds to barometric changes *earlier* than Port J, although Port L is deeper. This unexpected behavior was understood after measurements at Well 1015 and Well 1016, which extend into the basalt, revealed that the basalt has high permeability and is connected to the atmosphere at an unknown remote location. Thus, the subsurface pressure measurements reveal that the Bandelier Tuff is being ventilated both from ground surface and from the underlying basalt at this site. The tuff is also being ventilated from the exposed sides of the mesa. Thus, airflow within the mesa is in principle three-dimensional. However, at the interior locations of the monitor wells, the one-dimensional analysis presented below provided useful results.

Fig. 3b presents the amplitudes of the periodic atmospheric components as transformed from a 64-day window of data containing the short interval shown in Fig. 3a. The atmospheric S-tides, with periods of 1 day and all harmonics to 1/6 day, are evident. Fig. 3b is typical of the local barometric spectrum, except that the 1-day component sometimes has an amplitude somewhat closer to 1 mb (100 Pa). In Fig. 3b, each output period of the FFT is shown as a point connected to the horizontal axis to emphasize that it is inappropriate to draw a smooth curve between the points. The measured data points in the time domain can be exactly reconstructed from the FFT amplitudes and phases. Mathematically, for this data window and sampling interval, no other spectral components exist. If, for example, the FFT components were applied in calculating the flow of air into and out of ground surface, the calculated flow would be a complex sum dependent upon these unique components. An integral could be used only if the spectrum were converted to a continuous spectral density function.

5. Pressure transmission in Bandelier Tuff

5.1. Permeability measurements

Fig. 4 presents permeability as measured by the straddle packer apparatus in the four wells extending from the mesa top. As will be shown subsequently, vertical variations in permeability generally correlate with stratigraphy, although the peak values measured in Well 1002 and Well 1006 may represent intersections of these slanted wells with fractures.

5.2. Well 1004

Data of Well 1004 will be presented in detail to illustrate the analytical process. An abbreviated presentation will be presented for wells 1002, 1003, and 1006. Fig. 5a–d shows the measured values of amplitude ratio and phase shift at Well 1004 for periods of 8, 5.33, 1.0, and 0.5 days as points joined by solid curves, which may be compared with calculated values shown as dashed curves. The dashed curves represent the results of the one-dimensional analytic model in which one hypothetical subsurface layer represented by Eq. (4) corresponds to each measured value of permeability. Each hypothetical layer was extended either to an adjacent stratigraphic boundary or midway to the depth of the next permeability measurement. Fig. 5a and c compares the measured amplitudes and phase shifts with the predictions of Model "M", which used the *measured* values of permeability and porosity. (Because no porosity measurements were obtained from Well 1004, values from nearby Well 1003 were used.) Fig. 5b and d compares the measured amplitudes and phase shifts with predictions of "Model A", in which the values of permeability and porosity were *adjusted* by a trial-and-error procedure until a better agreement with data resulted.

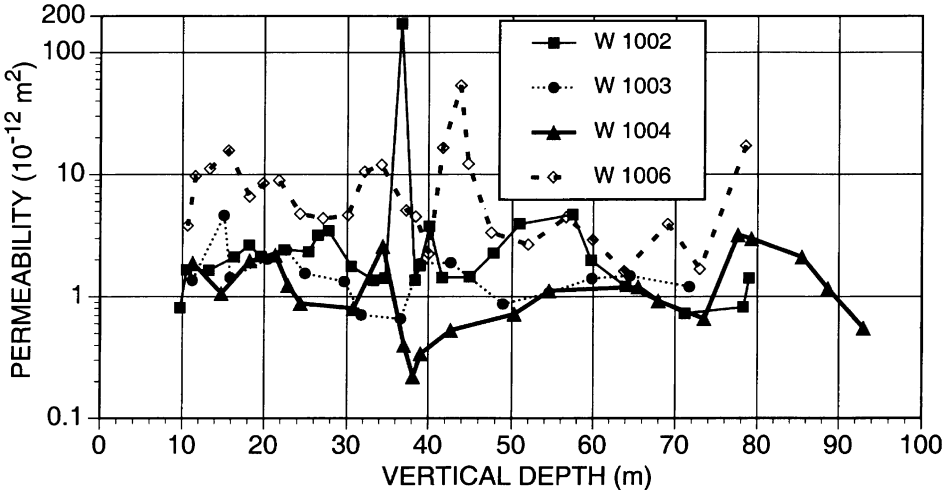

Fig. 4. Permeability versus depth at four wells as measured in situ by the straddle packer apparatus.

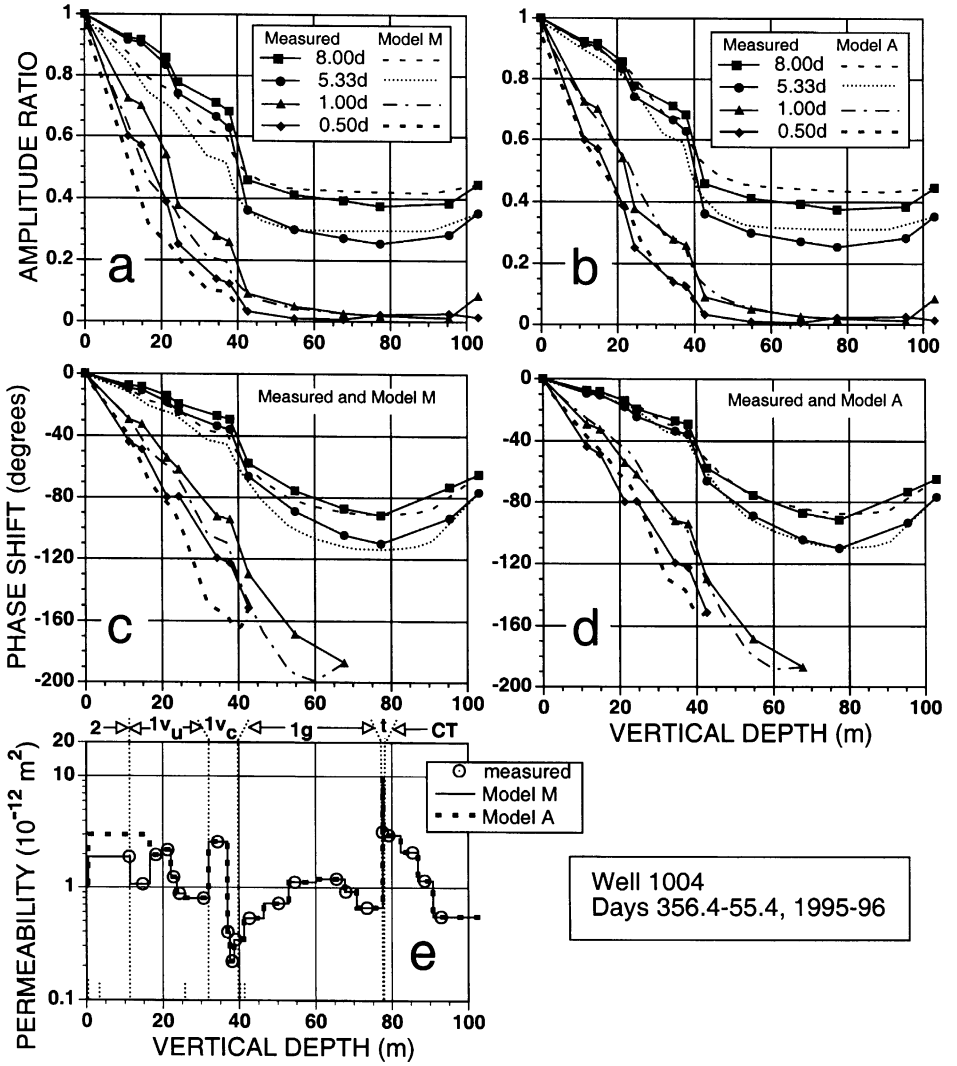

Fig. 5. Amplitude ratios (a and b), and phase shifts (c and d) versus depth at Well 1004 for four periods. The solid curves with points present measured data; the dashed lines present calculations by Model M and Model A, which used the measured and adjusted values of permeability, respectively. (e) Permeability versus depth.

The resolution of the absolute pressure transducer was 0.01 mb (1 Pa). The phases of components with amplitudes less than approximately five times the resolution, or 0.05 mb (5 Pa) are uncertain. Therefore, for each periodic component, the lower boundary condition of the analytic model was set to the measured amplitude and phase at the deepest port with an amplitude greater than 0.05 mb. Accordingly, the 1-day and 1/2-day model curves in Fig. 5a–d terminate at depths where the amplitude becomes less than 0.05

mb, and the measured phases of these components are not shown at greater depths in Fig. 5c and d.

Fig. 5e displays the permeability values in the context of stratigraphic boundaries, which are indicated by dotted vertical lines. Short dotted vertical lines indicate minor stratigraphic boundaries. To obtain the agreement of Model A with measurement shown in Fig. 5b and d, the only adjustment was to increase the permeability above the measured values in Qbt2 and at the top of $Qbt1v_u$, where fractures are known to exist.

In Fig. 5e, note that $Qbt1v_c$ contains an upper interval with a measured permeability of approximately 3×10^{-12} m^2, and a lower interval with permeability an order of magnitude smaller. These permeability values are associated with the relatively shallow slopes of the amplitude ratio and phase shift curves of Fig. 5a–d at 35-m depth, and the steep slopes at 40 m. As presented below, these graphic features become exaggerated at wells 1002, 1003, and 1006. When the initial pressure measurements in Well 1004 indicated little disagreement with the values of permeability as measured by the straddle packer, it was concluded that vertical fracture flow did not occur in the mesa in units other than Qbt2. Pressure measurements in the other wells subsequently demonstrated that this conclusion was erroneous.

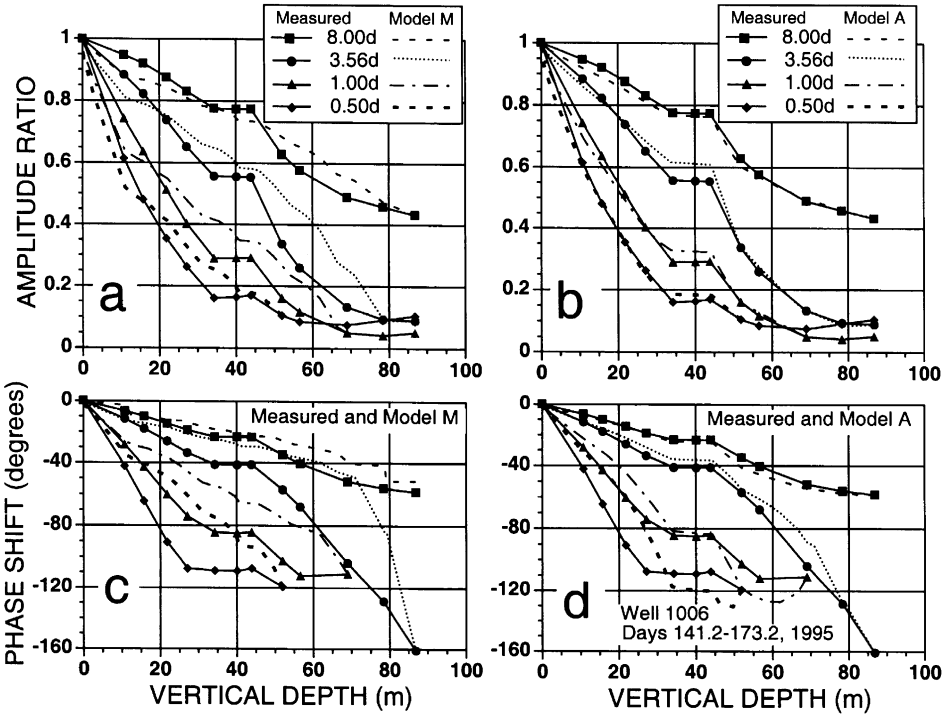

Fig. 6. Amplitude ratios (a and b), and phase shifts (c and d) versus depth at Well 1006, for four periods. Model A provides much better agreement of calculation with measured values. This is similar to results found at Well 1002 and Well 1003.

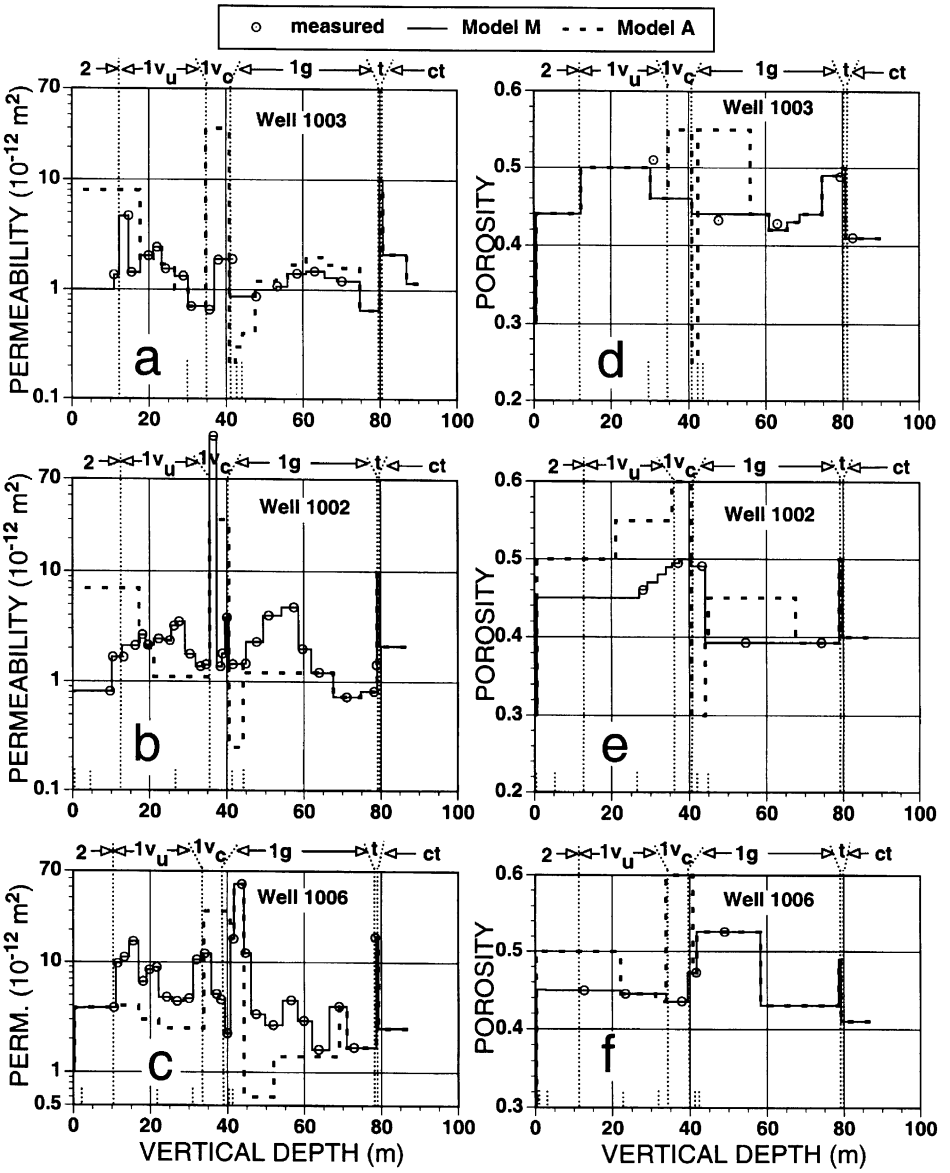

Fig. 7. Permeability and porosity versus depth. Measured values are shown as points. Model M is shown as solid lines, and Model A is shown as dashed lines. Stratigraphic contacts are indicated by vertical dotted lines. Minor subunits are indicated by short vertical dotted lines above the horizontal axis of each graph.

5.3. Wells 1002, 1003, and 1006

Fig. 6a–d presents the measured and calculated amplitude ratios and phase shifts at Well 1006, which is typical of the behavior observed at Wells 1002 and 1003. The three data points centered at 40-m depth indicate an interval of very small impedance, corresponding to the interval near 35 m in Well 1004. Unit $Qbt1v_c$ extends from approximately 34- to 39-m depth. The low-impedance interval extends to 44 m, indicating that $Qbt1v_c$ is fractured vertically, and that the fractures extend into the top of Qbt1g, as was described in the geologic summary of Section 2 above.

Fig. 7a–f presents the measured values of permeability and porosity as used in Model M, and the adjusted values used in Model A for each of these wells. In Well 1006, the adjusted permeability in and immediately below $Qbt1v_c$ is a factor of 3 to 10 larger than measured values. In all three wells, the adjusted permeability in $Qbt1v_c$ is much larger than measured, and the adjusted permeability near the top of Qbt1g is much smaller than measured. This suggests the presence of open vertical fractures in the interval of increased permeability, and the possibility of filled fractures or pores immediately below this interval. The difference between the dashed and solid curves of Fig. 7a–c indicates that the vertical permeability is quite different from the value measured by the straddle packer, which accents the horizontal permeability. Thus, the measurement of barometric pressure components revealed unexpected transport properties of the rock.

6. Factors confounding the interpretation

The interpretation of subsurface pressure data is fundamentally an inverse problem in a diffusive system, which can be confounded by several factors.

6.1. The ill-posed inverse problem

Deriving values for permeability and porosity from the pressure data constitutes an ill-posed inverse problem for which a unique solution is not possible. For example, from data at four particular frequencies, one can in principle solve for the permeability and porosity at each layer between measuring points. However, any small error in the data grows as a solution is obtained for successive layers, rapidly leading to unphysical results. Furthermore, the assumption of single values for permeability and porosity within a hypothetical layer is itself an approximation. Mathematically, a single lumped-parameter hypothetical layer cannot duplicate the pressure transmission of a physical interval that has varying properties. The trial-and-error search for an approximate solution in the model calculations reported here was adequate for revealing the gross properties of the different strata, because the permeability measurements provided good initial values in many intervals, and because informed judgment could be applied in the procedure. For a better estimate of the subsurface properties, one should employ an optimization procedure (Beck et al., 1985).

The methods used by Weeks (1978), Shan (1995), Ahlers et al. (1999), and Rousseau et al. (1999) all used iterative methods to select a presumed best match between the pressure

data and the inferred values of the soil properties. All of these methods are based on a transient solution of the pressure diffusion equation (Eq. (1)), whereas this paper utilizes harmonic analysis. The transient solutions can be used with a shorter time sequence of data than the harmonic solutions. However, the amplitudes and phase shifts of harmonic analysis may permit comparisons of theory with measurement, exemplified by Figs. 5 and 6, that can be interpreted more intuitively than comparison of pressure–time curves, such as Fig. 3a, with the corresponding results of calculations.

6.2. Pore moisture

The pressure data reported here were obtained during continual monitoring throughout 32- or 64-day windows of time. In principle, infiltration of moisture during monitoring could cause variation of air permeability and air-filled porosity, invalidating the interpretation. However, the climate is arid, snow depth rarely exceeds a few centimeters at the site, and rain evaporates quickly. Chloride mass balance in this mesa indicates moisture residence times within the mesa of thousands of years (Newman et al., submitted for publication). At some depths, the hydraulic gradient is such as to support upward unsaturated flow (Neeper and Gilkeson, 1996). Therefore, it is reasonable to assume that moisture throughout a significant interval of depth changed little during any particular data window.

6.3. Scale effect of permeability

The calculation used the same value of permeability for all periods, which may not correspond to reality. In heterogeneous materials, permeability is a scale-dependent property, in which the average permeability changes with sampling length due to the varying probability of including channels or voids within the sampled volume (Garbesi et al., 1996). The vertical propagation of a periodic component in effect samples the permeability over a horizontal extent of a fraction of the wavelength. In most intervals of Bandelier Tuff, the wavelength of a 1-day component is approximately 100 m. Therefore, it is possible that horizontal heterogeneity over distances of a few tens of meters within a stratigraphic unit could influence the measured amplitude and phase of the propagated pressure, and cause the type of discrepancies between the Model A calculation and measurement seen in Fig. 6. In general, it was noted that the discrepancy between calculation and measurement increased as the period (wavelength) became shorter, and therefore became potentially more sensitive to small inhomogeneities.

6.4. The Tsankawi pumice

In measuring permeability, the straddle packer apparatus applied a pressure to a vertical interval of 0.6 m. In any particular well, the apparatus may not have been centered on the Tsankawi pumice, resulting in an artificially small value for the measured permeability of that unit. Consequently, the Tsankawi pumice was assigned a permeability of 10×10^{-12} m^2, in all wells except Well 1006, where the measured value was 20×10^{-12} m^2. This unit is so thin that it had little influence on the calculated one-dimensional vertical pressure

propagation in the layer model. However, rapid propagation of vacuum in this unit during active extraction tests, and scatter appearing in the measured pressure spectrum at this unit, are consistent with a hypothesis in which that unit rapidly transmits pressures horizontally over distances greater than the separation between wells. Therefore, the propagation of barometric variations may not be strictly one-dimensional through the Tsankawi pumice. If so, the shorter wavelengths would be affected most. The shorter wavelengths are more sensitive to soil properties, and will have the greatest differences of phase and amplitude at the same stratum in different wells. Therefore, the measured amplitude and phase of a shorter wavelength component (such as the 1-day component) at the Tsankawi pumice may not be consistent with measurements of the same component above and below this stratum.

6.5. Artificial pressure signals

Pressure components with prominent amplitudes at ground surface were selected for comparison of measurements with models. The analysis assumes that no nonlinear frequency-shifting processes occur in the ground. In addition, the analysis assumes that no artificial periodic signals enter the measurements. It was necessary to maintain the transducers at constant temperature to avoid an artificial 24-h signal resulting from the ambient diurnal temperature cycle.

As atmospheric pressure rises or falls, the pressure in the retractable membrane liner of a well must also rise or fall with an amplitude and delay, which are dependent upon the volume of the liner and the characteristics of the air pump. For example, the estimated amplitude ratios of the pressure in the membrane are 0.4 and 0.7 for periods of 1 and 2 days, respectively. The estimated corresponding phase shifts are $-63°$ and $-45°$, respectively. A subsurface leak from the membrane would cause a vector addition to the observed pressure at a port near the leak. No anomalous behavior was noted at any particular port of wells reported here. The conclusions regarding the vertical permeability of $Qbt1v_c$ are based on data from three different wells, and therefore are not due to a leak in a membrane.

7. Pressure transmission in the basalt

Two nearly parallel boreholes were drilled with an air rotary rig into the basalt from the north side of the mesa at dip angles near 60° from horizontal. These were completed as permanent monitoring wells 1015 and 1016. During drilling of Well 1016 in the basalt, return air was lost and air emerged from the then partially backfilled Well 1015, indicating a high-permeability connection between the wells.

7.1. Variation of pressure with depth

Fig. 8 presents pressure as a function of time for the atmosphere and the seven ports in Well 1015. The ports are labeled A through G in order of depth as shown in Fig. 1. Ports D, E, F, and G are in the basalt. In Well 1015, Port A is at the Qbt1v–1g contact, Port B is

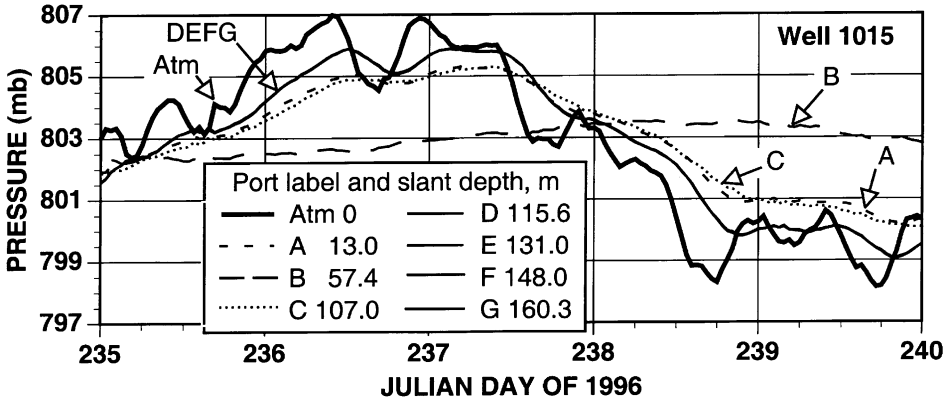

Fig. 8. Pressure versus time at ground surface and at seven depths of Well 1015. Pressures at ports D, E, F, and G, which are in the basalt, differ by less than the width of the curve.

in the Tsankawi pumice, and Port C is at the bottom of the Guaje pumice bed, immediately above the 2.2 m of moist silt that lies on top of the basalt at this location. In Fig. 8, the pressures at Ports D–G differ by less than the width of the curve. The pressure in the basalt follows the atmospheric pressure more closely than the pressure at Port A, which is 13 m from ground surface along the axis of the borehole. The difference of pressures between Port C and Ports D–G suggests that the silt layer provides significant impedance at this location, although it may exist only in local depressions in the basalt surface. The silt layer is only 0.5 m thick at Well 1016, where the top of the basalt is at an elevation 10 m higher than at Well 1015.

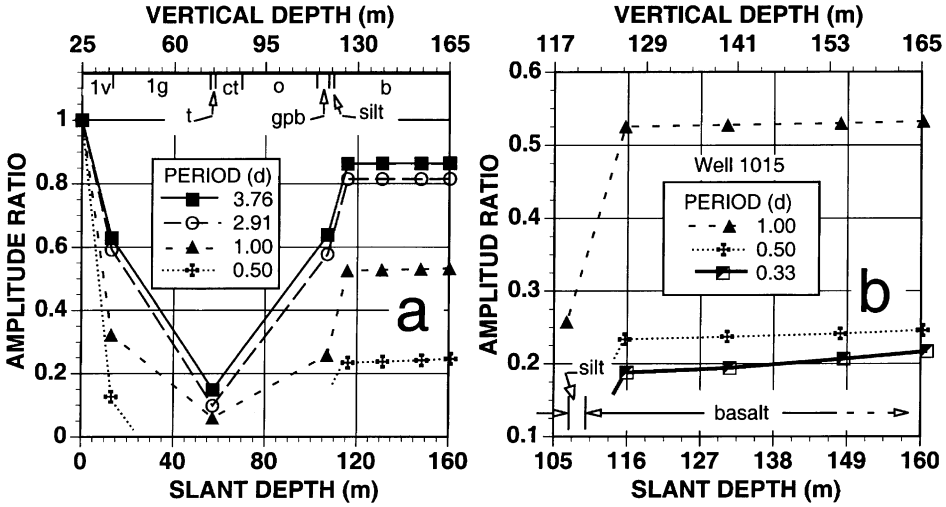

Fig. 9. (a) Amplitude ratio versus slant depth from the wellhead and vertical depth below the mesa surface. (b) Detail of amplitude ratio versus depth in the basalt, indicating an increase of amplitude with depth.

Fig. 9a presents the amplitude ratios of selected prominent components as functions of depth in Well 1015. The amplitude attenuation through the silt is clearly evident. Fig. 9b presents detail of the amplitude ratios in the basalt. The slight attenuation with decreasing depth is evident, particularly for the 0.5- and 0.33-day components, although these small changes are beyond the resolution of the transducers. This attenuation suggests that the pressure propagates in a direction with a component upward along the axis of the borehole. Therefore, the pressure is propagated either from below Port G, or from a southern or easterly direction.

7.2. Frequency dependence of pressure propagation

Fig. 10 presents the amplitude ratios and phase shifts at Ports G of Wells 1015 and 1016, together with curves predicted by two different models. The "infinite depth" model simulates the basalt as a one-dimensional channel of infinite length, filled with a porous medium, in which the amplitude attenuation and phase shift are given by Eq. (3). The infinite depth model predicts that, at any particular location within the medium, the amplitude ratio would vary exponentially as a constant divided by the square root of the period, and the phase shift would be proportional to this same quantity. The dashed lines in

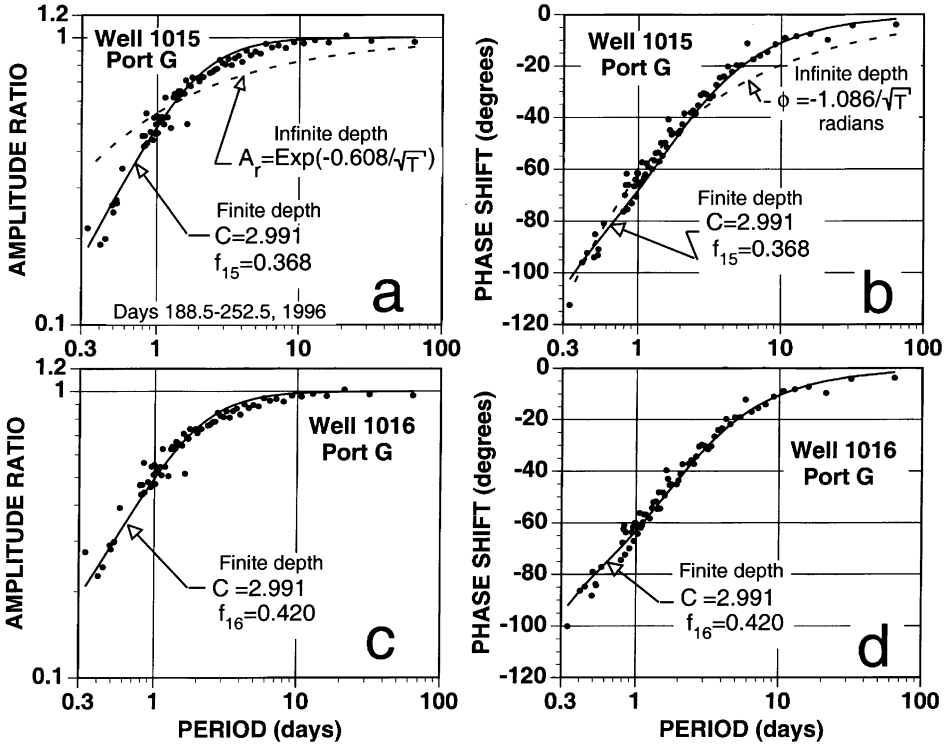

Fig. 10. (a and b) Amplitude ratio and phase shift at Port G of Well 1015, compared with results of the infinite depth and finite depth models. (c and d) Amplitude ratio and phase shift at Port G of Well 1016, compared with the finite depth model.

Fig. 10a and b indicate that the infinite depth model provides a poor fit to the data of Well 1015. Furthermore, the amplitude and phase shift should have the same value of the constant, which is not true in the fits to the data presented by the dashed curves in Fig. 10a and b.

The solid curves in Fig. 10 represent the data as fit to a "finite-depth" model, illustrated schematically in Fig. 11. In this model, the basalt is represented as a one-dimensional channel of length L, containing a uniform porous medium, with an impermeable end. The amplitude ratio and phase shift, at a location fL from the closed end of the medium, are given by the complex expression (Carslaw and Jaeger, 1959, p. 105)

$$\mathbf{A}_{\mathrm{r}} = \frac{\cosh[\beta L f(1+i)]}{\cosh[\beta L(1+i)]}. \tag{5}$$

The dependence of Eq. (5) on the period is made explicit by representing the decay parameter, β, as

$$\beta L = \frac{C}{2\sqrt{T}}\ , \tag{6}$$

in which T is the period and C is a constant of the medium:

$$C = 2L\sqrt{\frac{\pi\mu\theta}{kP_{00}}}\ . \tag{7}$$

The amplitude ratio, which is the magnitude of Eq. (5), is

$$A_{\mathrm{r}} = |\,\mathbf{A}_{\mathrm{r}}\,| = \left[\frac{\cosh\left(\frac{C}{\sqrt{T}}f\right) + \cos\left(\frac{C}{\sqrt{T}}f\right)}{\cosh\left(\frac{C}{\sqrt{T}}\right) + \cos\left(\frac{C}{\sqrt{T}}\right)}\right]^{\frac{1}{2}}\ . \tag{8}$$

The tangent of the phase shift is the ratio of imaginary to real parts of Eq. (5). The values of C, f_{15}, and f_{16} were obtained by fitting the data to Eq. (8) and to the

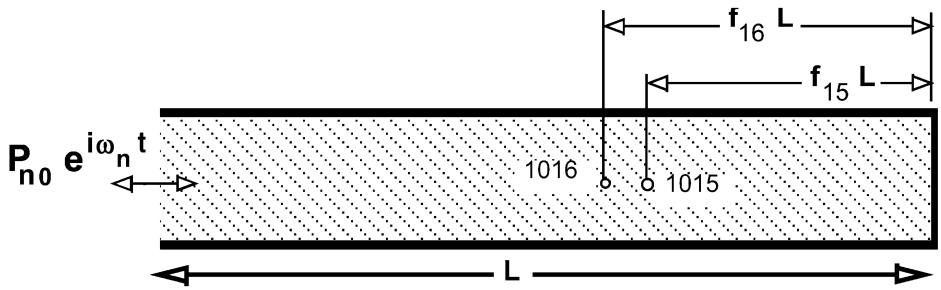

Fig. 11. Conceptual diagram of the finite depth model. The location of Wells 1015 and 1016 are shown relative to the impermeable end of a matrix-filled channel.

corresponding phase expression, while requiring the same value of C for both wells. As shown in Fig. 10, the finite-depth model closely fits the data of each individual well. Good fits to the data could be obtained while the value of C varied $\pm 10\%$ and the corresponding values of f_{15} and f_{16} varied in the range 0.3–0.5. However, the difference $(f_{16} - f_{15})$ remained nearly constant in the range 0.05–0.06. This behavior lends some credence to the model, because the difference $(f_{16} - f_{15})$ represents the fraction of the length of the hypothetical channel occupied by the distance between the wells, and therefore should be constant.

7.3. Well-to-well comparisons

Port G of Well 1015 experiences nearly the same pressure as Port G of Well 1016, with the pressure at Well 1015 being slightly more attenuated and delayed than that at Well 1016. Because Well 1016 is southeast of Well 1015, the pressure difference suggests that the origin of pressure is to the southeast of the two wells. Expressions similar to Eq. (5) or Eq. (8) can be applied to the ratio of amplitudes at the two wells, A_{r15}/A_{r16}, and to the phase difference between the wells, $\phi_{15} - \phi_{16}$. Fig. 12 shows the results. The measured phase difference of $-2°$ for the 1-day period is equivalent to an 8-min time interval for propagation of that component across the 128-m distance between the wells. The values of C, f_{15}, and f_{16} were also varied in an attempt to make the finite depth model fit the well-to-well data of Fig. 12, but the most satisfactory simultaneous fit to both amplitude ratio and phase was provided by the parameters as shown in Fig. 10. In Fig. 12, the disagreement of the model with the well-to-well amplitude ratio and phase difference is not surprising. The model assumes one-dimensional pressure propagation in a uniform medium, whereas the actual medium is heterogeneous, and the flow is probably three-dimensional.

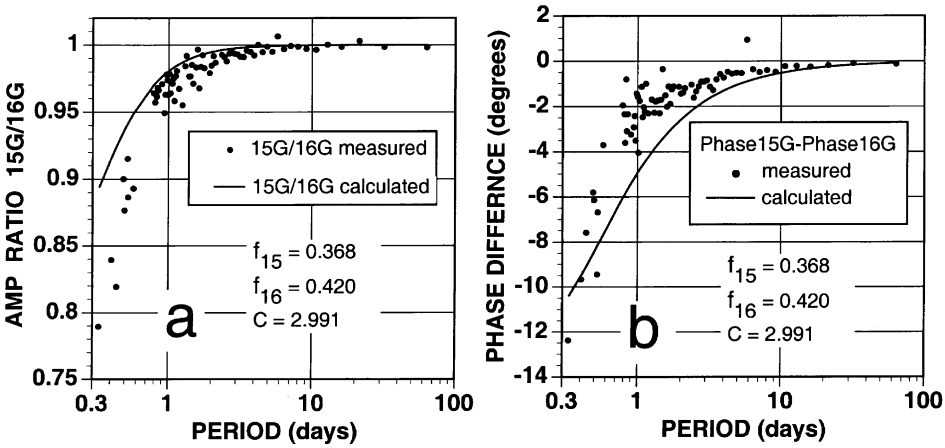

Fig. 12. (a) Ratio of amplitude at Well 1015 to amplitude at Well 1016. (b) Phase at Well 1015 minus phase at Well 1016. Points represent measured data. The solid curves represent calculated values according to the finite depth model.

7.4. Estimated transport characteristics of the basalt

The values of C, f_{15}, and f_{16} permit quantitative estimates of the basalt properties, within the limits of the one-dimensional model. The distance between Ports 15G and 16G is approximately 128 m. From

$$f_{16}L - f_{15}L = 128 \text{ m}, \tag{9}$$

the model predicts that L is approximately 2.5 km, and that the wells are approximately 1.5 km from the open end of the channel. A hole in an outcrop of the basalt, known as "wind cave", is located in a shallow canyon approximately 3.8 km southeast of the site in the general direction of the azimuth connecting the wells. This may be the atmospheric vent for the basalt at the site. However, the tuff is not present and only a thin soil remains on top of the basalt at distances greater than 3 km southeast of the site, so the basalt might be ventilated at any of many locations. The idealized model leading to Eq. (9) enables only an order-of-magnitude prediction. Because the prediction is of the same magnitude as the observed distance to potential ventilation sites, the model may be regarded as having some validity.

Combining the values of C and L with Eq. (7) provides a numerical value for k/θ, approximately 2.2×10^{-8} m^2. For porosity in the range 0.1–0.5, the permeability would be in the range 2×10^{-9}–1×10^{-8} m^2, that is, greater than 1000 darcies.

8. Conclusions

The penetration of barometric pressure variations provides a useful tool for diagnosis of gas flow in the subsurface, particularly when the data are expressed in the frequency domain. In the present case, the measurements provide strong evidence for vertical fracture flow in the "colonnade" subunit (Qbt1v_c), and reveal the characteristics of the unexpected connection of the underlying basalt with the atmosphere. Extension of the frequency domain analysis to quantitative prediction of flow in open boreholes and passive soil vapor extraction will be presented in a subsequent paper.

Notation

A_r	Amplitude magnitude ratio, usually relative to atmospheric amplitude.
$\mathbf{A}_\text{r}$	Complex amplitude ratio.
C	A constant of the soil properties.
$\mathbf{C}_1$,$\mathbf{C}_2$	Complex constants from boundary conditions.
f_{15}	Fraction of L between Well 1015 and the impermeable end of the medium.
f_{16}	Fraction of L between Well 1016 and the impermeable end of the medium.
i	$\sqrt{-1}$.
k	Air permeability.
L	Length of a one-dimensional region.
n	Subscript denoting a frequency component.
P	Pressure.

P_{00}	Time-averaged atmospheric pressure (at zero frequency, zero depth), approximately 80,000 Pa at the site.
P_n	Amplitude of pressure in the subsurface at frequency ω_n.
$\mathbf{P}_n$	Complex component of pressure in the subsurface at frequency ω_n.
P_{n0}	Amplitude of atmospheric pressure (zero depth) component at frequency ω_n.
T_n	Period of oscillatory pressure, $2\pi/\omega_n$.
t	Time.
y	Depth below ground surface or within a layer.
β	Exponential factor for pressure attenuation.
θ	Air-filled porosity.
μ	Viscosity of air.
ϕ	Phase, phase shift, or phase difference.
ϕ_{15},ϕ_{16}	Phase of pressure components at Port G of Well 1015 or Well 1016.
ω	Angular frequency.

Acknowledgements

The Los Alamos National Laboratory supported all field work preceding the analysis. R. Gilkeson supervised the field work. Wm. Lowry supervised the permeability measurements. S. Limback constructed the pressure measuring apparatus and obtained data. K. Kisiel and T. Renn assisted with data acquisition and reduction.

Appendix A. Data reduction

Within any chosen window of time, the atmospheric and subsurface pressure data were transformed to a real Fourier series

$$P(t) = P_{00} + \sum_n P_{n0}\cos\left(\frac{2\pi}{T_n}t + \phi_n\right), \tag{A1}$$

in which the time was arbitrarily referenced to zero at solar midnight in the middle of the data window. The quantities of interest are amplitude ratios and phase shifts at depth, at any particular period, T_n:

$$A_{\mathrm{r}} = \frac{P_n(y)}{P_{n0}(y=0)}; \qquad \text{ph shift} = \varphi_n(y) - \varphi_n(y=0). \tag{A2}$$

In effect, the Fourier transform corresponds to a repeating series of identical windows in time, each containing the same function $P(t)$, as shown in Fig. 13. Therefore, care in selection of the data window is required. In the transformed data, the pressure in the days immediately prior to the window would in effect be the same as the pressure during the last days of the window. As shown in Fig. 13c, selection of "bad window" would generate results as though the pressure were discontinuous at the beginning of the window. Some

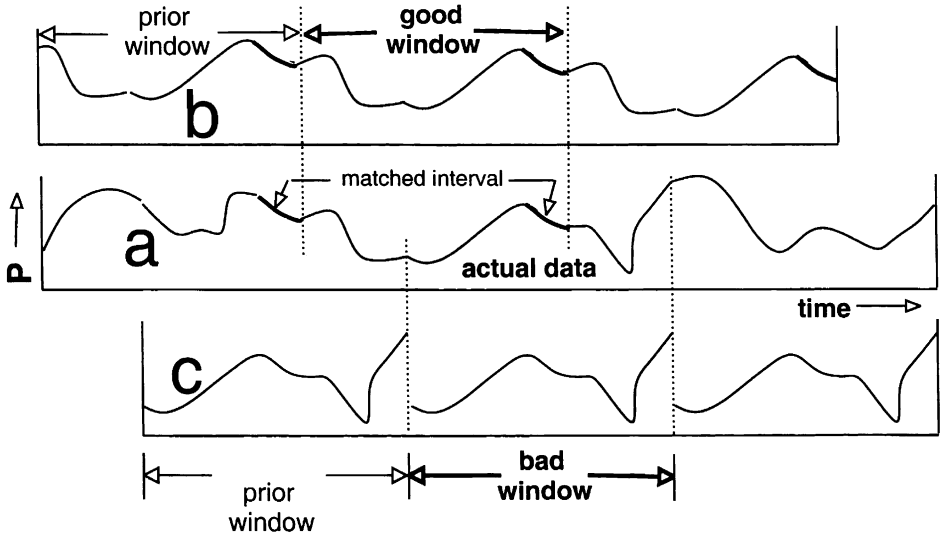

Fig. 13. Conceptual illustration of window selection. (a) Actual data versus time. (b) A good repeating window as implicit in the FFT, in which data immediately prior to the window match the data at the end of the window. (c) A bad repeating window as implicit in the FFT, in which data do not match at window edges.

workers use "windowing" techniques to de-emphasize data near the window boundaries (Ramirez, 1985). In the work reported here, a computer routine selected the window in which the atmospheric pressure history during the last 2 days of the window differed minimally from the history during the 2 days immediately prior to the window. This is illustrated in Fig. 13b by the "good window", which is selected to terminate at the end of the "matched interval" in the actual data of Fig. 13a. For data analysis and model calculations, this window selection provides a correct cause for all subsurface effects that occur within 2 days of any change of atmospheric pressure. Even at depths in the tuff exceeding 100 m, the influence of a barometric change at ground surface has decayed to minor significance after 2 days. Stated in other terms, pressure variations can be regarded as packets of waves transmitted through the ground. For pressure in a porous medium, the group velocity of a packet happens to be twice the phase velocity of an individual harmonic component. In a medium with the permeability and porosity of Bandelier Tuff, the group velocity of a wave packet centered on a 10-day period is approximately 60 m/day, so even disturbances with long periods would reach depths of 100 m within 2 days. The careful selection of data windows, therefore, enables a proper relationship of cause and effect in the calculations.

References

Ahlers, C.F., Finsterle, S., Bodvarsson, G.S., 1999. Characterization and prediction of subsurface pneumatic response at Yucca Mountain Nevada. J. Contam. Hydrol. 38, 47–68.

Beck, J.V., Blackwell, B., St. Clair Jr., C.R., 1985. Inverse Heat Conduction Ill-posed Problems. Wiley, New York.

Broxton, D.C., Reneau, S.L., 1995. Stratigraphic nomenclature of the Bandelier Tuff for the Environmental Restoration Project at Los Alamos National Laboratory. Los Alamos National Laboratory report LA-13010-MS, available from National Technical Information Service, US Department of Commerce, 5285 Port Royal Rd., Springfield, VA 22161 USA.

Broxton, D.C., LaDelfe, C., Chipera, S.J., Kluk, E.C., 2000. Stratigraphy, mineralogy and chemistry of bedrock tuffs at Mesita del Buey, Los Alamos National Laboratory, New Mexico, In preparation. Report to be released.

Burkhard, N.R., Hearst, J.R., Hanson, J.M., 1987. Estimation of the bulk diffusivity of chimneys using post-shot holes. Proc. Fourth Symposium on Containment of Underground Nuclear Explosions, vol. 2. CONF-870961, Colorado Springs, CO, USA, Sept. 21–24, pp. 288–315.

Carslaw, H.S., Jaeger, J.C., 1959. Conduction of Heat in Solids, 2nd edn. Clarendon Press, Oxford.

Chapman, S., Lindzen, R.S., 1970. Atmospheric Tides. D. Reidel Publishing, Dordrecht, The Netherlands.

Ellerd, M.G., Massmann, J.W., Schwaegler, D.P., Rohay, V.J., 1999. Enhancements for passive vapor extraction: the Hanford study. Ground Water 37, 427–437.

Fukuda, H., 1955. Air and vapor movement in soil due to wind gustiness. Soil Sci. 79, 249–256.

Garbesi, K., Sextro, R.G., Robinson, A.L., Wooley, J.D., Owens, J.A., 1996. Scale dependence of soil permeability to air: measurement method and field investigation. Water Resour. Res. 32, 547–560.

Lewis, W.C., 1991. Atmospheric pressure changes and cave airflow: a review. National Speleological Society Bull. 53, 1–12.

Massmann, J., Farrier, D.F., 1992. Effects of atmospheric pressures on gas transport in the vadose zone. Water Resour. Res. 28, 777–791.

Neeper, D.A., Gilkeson, R.H., 1996. The influence of topography, stratigraphy, and barometric venting on the hydrology of unsaturated Bandelier Tuff. In: Goff, F. (Ed.), The Jemez Mountains Region: New Mexico Geological Society, Forty-Seventh Annual Field Conference. New Mexico Geological Society, Socorro, NM, USA, pp. 427–432.

Newman, B.D., Gallaher, B.M., Gilkeson, R.H., 2000. Novel hydrologic behavior of semi-arid mesas. In preparation.

Ramirez, R.W., 1985. The FFT Fundamentals and Concepts. Prentice-Hall, Englewood Cliffs, NJ, USA.

Robinson, A.L., Sextro, R.G., Riley, W.J., 1997. Soil-gas entry into houses driven by atmospheric pressure fluctuations—the influence of soil properties. Atmos. Environ. 10, 1487–1495.

Rojstaczer, S., Tunks, J.P., 1995. Field-based determination of air diffusivity using soil air and atmospheric pressure time series. Water Resour. Res. 31, 3337–3343.

Rousseau, J.P., Kwicklis, E.M., Gillies, D.C., 1999. Hydrogeology of the unsaturated zone, north ramp area of the Exploratory Studies Facility, Yucca Mountain, Nevada. US Geological Survey Water-Resources Investigations Report 98-4050. Available from: US Geological Survey Information Services, Box 25286, Federal Center, Denver, CO 80225 USA. Also available on the internet at http://m-oext.ymp.gov/html/prod/rms/MOL199904190335.HTM.

Shan, C., 1995. Analytical solutions for determining vertical air permeability in unsaturated soils. Water Resour. Res. 31, 2193–2200.

Weeks, E.P., 1978. Field determination of vertical permeability to air in the unsaturated zone. US Geological Survey Professional Paper 1051, available from the Superintendent of Documents, US Government Printing Office, Washington, DC 20402 USA. Stock Number 024-001-03092-6.